applied nano

MDPI

Article

Sildenafil-Coated Silver Nanoparticles for Anal Fissure Wound Healing—A Combined Experimental/Molecular Docking Study

Mahboubeh Dolatyari [1,2], Parisa Rostami [3], Mahsa Hejazad [3], Ali Rostami [1,2,4,5,*], Manouchehr Khoshbaten [3], Mahdi Dolatyari [6], Hamit Mirtagioglu [7] and Axel Klein [8,*]

1 SP-EPT Lab., ASEPE Company, Industrial Park of Advanced Technologies, Tabriz 5364191686, Iran; mdolatya@uni-koeln.de
2 Next Matter Nano Tech Lab, NAREKS Company, 09900 Nazilli, Türkiye
3 Faculty of Medicine, Tabriz University of Medical Science, Golgasht Street, Tabriz 516615731, Iran; parisarst99@gmail.com (P.R.); mhhejazad@gmail.com (M.H.); khoshbatenm@tbzmed.ac.ir (M.K.)
4 Photonics and Nanocrystal Research Lab. (PNRL), University of Tabriz, Tabriz 5166614761, Iran
5 Electrical and Electronics Engineering Department, Ege University, 35040 Izmir, Türkiye
6 Department of Pharmacology, University of Arizona, University Boulevard, Tucson, AZ 85724, USA; mahdid@arizona.edu
7 Department of Statistics, Faculty of Science and Literature, University of Bitlis Eren, 13000 Bitlis, Türkiye; hmirtagioglu@beu.edu.tr
8 Institute for Inorganic and Materials Chemistry, Department of Chemistry and Biochemistry, Faculty of Mathematics and Natural Sciences, University of Cologne, Greinstraße 6, D-50939 Cologne, Germany
* Correspondence: rostami@tabrizu.ac.ir (A.R.); axel.klein@uni-koeln.de (A.K.)

Abstract

PVP-stabilized silver nanoparticles (Ag NPs) were functionalized with sildenafil (Sil), leading to spherical NPs (Ag@Sil NPs) with a size of about 30 nm as observed through transmission electron microscopy and dynamic light scattering. Fourier-transformed IR spectroscopy confirmed the covering of the particles with Sil. The Ag@Sil NPs were incorporated into a 0.1 wt% ointment and tested for the treatment of acute anal fissures in a preliminary medical study involving 50 patients. Typical symptoms such as pain, bleeding, itching, and mass sensation were improved in the intervention group with no adverse effects. Molecular docking showed strong interactions with docking scores slightly above −10 kcal/mol between sildenafil and two different model complexes $[Ag–Sil]^+$ for the Ag-bound sildenafil with either piperazine-N- or pyrazole-N-bound Ag^+ ions and the muscarinic M2 and the nicotinic acetylcholine α3β4 receptor, which are both involved in anal sphincter regulation. All three showed superior binding compared with nitroglycerin and *L*-arginine. The residue analysis revealed a higher number of relevant interactions for the sildenafil and the two Ag^+ complexes, compared to nitroglycerin and *L*-arginine, fully in line with the differences in the docking scores.

Keywords: silver nanoparticles; sildenafil; molecular docking; topical therapy; anal fissure

Check for updates

Academic Editors: Neeraj Chauhan and Pallabita Chowdhury

Received: 8 April 2026
Revised: 27 May 2026
Accepted: 13 June 2026
Published: 19 June 2026

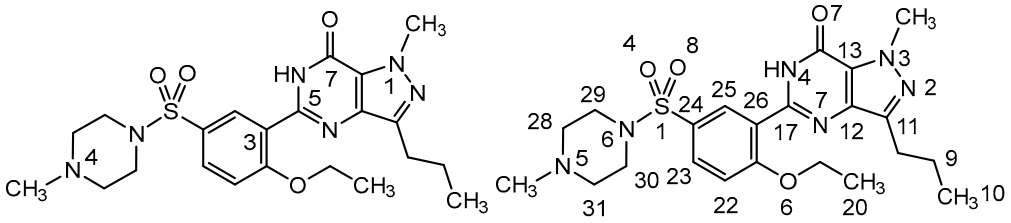
Copyright: © 2026 by the authors. Licensee MDPI, Basel, Switzerland. This article is an open access article distributed under the terms and conditions of the Creative Commons Attribution (CC BY) license.

1. Introduction

Silver nanoparticles (Ag NPs) have attracted attention for their antimicrobial, antiviral, antifungal, anti-inflammatory, and wound-healing properties, especially when functionalized with bioactive ligands [1–12]. Multiple studies show that Ag NPs act as drug delivery platforms while also contributing antibiotic properties—a dual-mode action also used in other NP systems [1–4,6,7,9,12–16].

We selected Ag NPs as a delivery platform for sildenafil with the aim of treating anal fissures through such a dual-mode action. Anal fissures are common anorectal lesions

that, when chronic, are complicated by impaired healing, localized ischemia, and internal anal sphincter (IAS) hypertonia [17–19]. Recent reports emphasize that impaired wound-healing in chronic anal fissures (CAF) may be mediated not only by mechanical trauma but also by inflammatory microenvironments and neurochemical imbalances that sustain sphincter spasm and pain [19–21]. Targeting IAS relaxation and local tissue recovery is thus a central scientific strategy in non-surgical management [18,19,21–23]. Sildenafil (Scheme 1), a phosphodiesterase type 5 (PDE5) inhibitor, is known to enhance cyclic GMP signaling and smooth muscle relaxation [24–29]. While the activity of sildenafil on PDE5 has been extensively studied, including molecular docking and molecular dynamics studies, recent interest has emerged in evaluating its potential off-target effects on other receptor classes [30–35]. However, to date, no docking studies have investigated its interaction with cholinergic receptors such as the M2 muscarinic or α3β4 nicotinic acetylcholine receptors, which are key receptors in parasympathetic regulation of anal sphincter tone. Similarly, nitric oxide donors like *L*-arginine and nitroglycerin, despite their known therapeutic use in anal fissure, have not been explored for their molecular binding affinity to these receptor systems.



Scheme 1. Chemical structure of sildenafil (1-{[3-(1-methyl-7-oxo-3-propyl-6,7-dihydro-1*H*-pyrazolo[4,3-*d*]pyrimidin-5-yl)-4-ethoxyphenyl]sulfonyl}-4-methylpiperazine) with partial numbering. (**Left**) official numbering in selected groups, (**Right**) our numbering.

In this study, sildenafil-modified silver nanoparticles (Ag@Sil NPs) were prepared and characterized. The idea was to use Ag for local antimicrobial effects and sildenafil for smooth muscle relaxation via receptor-mediated pathways in a dual-mode action as described above. An ointment containing 0.1 wt% of the NPs was used in preliminary clinical trials for the treatment of both infected and non-infected anal fissures. A molecular docking study of the nicotinic acetylcholine α3β4 and the muscarinic M2 receptors, using two different molecular $[Ag–Sil]^+$ models for the Ag@Sil material, was carried out in comparison to the established nitric oxide donors *L*-arginine and nitroglycerin.

Although sildenafil has been extensively studied as a PDE5 inhibitor, with numerous molecular docking studies confirming its high-affinity binding to PDE5 and related enzymes [36–39], very few works have extended such investigations to non-canonical targets. A handful of in silico studies have examined its interaction with proteins such as NF-kB (Nuclear Factor kappa-light-chain-enhancer of activated B-cells), HMGB1 (High-Mobility Group Box 1), or steroidogenic receptors, primarily to explore anti-inflammatory or reproductive applications [30–35]. However, no docking studies have been reported so far with muscarinic or nicotinic acetylcholine receptors, which are key regulators of smooth muscle tone in the anorectal region. Likewise, nitroglycerin and *L*-arginine, despite their clinical relevance as nitric oxide donors, have not been assessed via docking against these cholinergic targets. To the best of our knowledge, the present study is the first to simulate and compare the binding profiles of sildenafil-covered Ag NPs, sildenafil, nitroglycerin, and *L*-arginine against both the M2 muscarinic and the α3β4 nicotinic acetylcholine receptor.

For our clinical study, the primary endpoint was explicitly defined as fissure healing based on clinical examination over a typical period of two weeks, as this represents the most objective and clinically relevant outcome reflecting therapeutic efficacy. Secondary

endpoints included pain reduction, bleeding, and other symptom-related improvements, which were evaluated to provide supportive evidence for the clinical benefit. We acknowledge that assessing multiple outcomes may increase the risk of multiplicity bias. However, the study was designed as an exploratory clinical investigation to evaluate the overall therapeutic potential and safety profile of the sildenafil-modified Ag NP ointment. Therefore, secondary endpoints were not independently powered but were included to capture the broader clinical response.

2. Materials and Methods

2.1. Materials

Silver nitrate ($AgNO_3$) (ReagentPlus, ≥99%), polyvinyl pyrrolidone (PVP) (ReagentPlus, ≥99%), sodium borohydride ($NaBH_4$) (ReagentPlus, ≥99%), dimethyl sulfoxide (DMSO) (ReagentPlus, ≥99%), sildenafil citrate ($C_{22}H_{30}N_6O_4SC_6H_8O_7$) (ReagentPlus, ≥98%), and Vaseline (®, ReagentPlus, ≥98%) were purchased from Aldrich, Merck, Darmstadt, Germany. Argan oil (ReagentPlus, ≥99%) was received from Bioadprates Product SARL, Agadir, Morocco, and used without further purification.

2.2. Preparation of the Sildenafil-Modified Ag Nanoparticles (Ag@Sil NPs)

Silver nanoparticles (Ag NPs) were synthesized by dissolving 0.5 g (3 mmol) of $AgNO_3$ and 1.5 g (0.15 mmol) of polyvinyl pyrrolidone (PVP) in 400 mL of deionized water and stirring for 5 min. A total of 0.11 g (3 mmol) of $NaBH_4$ at ambient temperature (25 ± 2 °C) and under ambient air was dissolved in 100 mL of deionized water and added dropwise to the initial solution under continuous stirring. The formation of Ag NPs was completed within 15–30 min, as indicated by a color change from colorless to yellow-brown. The resulting NPs were centrifuged at 12,000 rpm for 15 min and washed three times with 10 mL portions of deionized water and acetone. A total of 0.4 g of the PVP-coated NPs were dispersed in 40 mL of dimethyl sulfoxide (DMSO) using an ultrasonic bath. A total of 0.1 g (0.15 mmol) of sildenafil citrate ($C_{22}H_{30}N_6O_4SC_6H_8O_7$) was dissolved in 10 mL of DMSO and added to the NP suspension. The mixture was stirred overnight, after which it was centrifuged at 12,000 rpm. The obtained NPs were washed three times with deionized water and acetone. Elemental analysis was performed using energy-dispersive X-ray spectroscopy (EDX).

2.3. Instrumentation

Ultrasonic dispersion was achieved using a Sonorex Digitec DT ultrasonic bath (Bandelin, Berlin, Germany). For centrifugation a custom-built centrifuge manufactured by ASEPE Company (Asepe, Tabriz, Iran), with a maximum speed of 20,000 rpm, was used. Elemental analysis was obtained through energy-dispersive X-ray (EDX) spectroscopy using a CIQTEK EDAX-EDS instrument (CIQTEK, Hefei, Anhui, China) in combination with a scanning electron microscope (SEM) Tescan-Vega2 instrument (Tescan, Brno, Czech Republic). Transmission electron microscopy (TEM) was carried out using a Philips EM 208S instrument (Philips, Eindhoven, The Netherlands). Dynamic light scattering (DLS) was studied using a VASCO DLS system (Scimed, Stockport, UK). Fourier-transform infrared (FT-IR) spectra were recorded using an MB3000 spectrometer (ABB, Zürich, Switzerland). Powder X-ray diffraction was carried out using a Siemens D500 diffractometer with Cu-Kα radiation (λ = 1.541 Å) (Siemens, Bruker, Rheinhausen, Germany). UV–Vis absorption spectra were recorded using a PG Instruments Ltd. T70 UV–Vis spectrophotometer (PG Instruments, Lutterworth, UK).

2.4. Preparation of the Ointment

A total of 10 g of 1-hexadecanol, 5 g of argan oil, and 5 g of Vaseline were melted and mixed in a warm water bath (50–70 °C). Simultaneously, 0.2 g of the synthesized NPs were dispersed in 25 mL of DMSO and heated to 70 °C. The two liquids were combined and vigorously stirred while cooling down to room temperature. The final product had a cream-like texture and contained 0.1 wt% Ag@Sil.

2.5. DFT-Geometry Optimization on Model Compounds and Docking Study

Crystallographic information files (CIFs) of *L*-arginine [40], nitroglycerin [41], and sildenafil [42–46], were used as input for DFT-optimized structures. *L*-arginine was used in its zwitterionic form consistent with physiological pH conditions. In order to model the Ag@Sil material, two molecular model compounds, $[Ag–Sil(Pip)]^+$ and $[Ag–Sil(Pyz]^+$ were created and their structures optimized (data, see Tables S4 and S5 in the Supplementary Materials). In the $[Ag–Sil(Pip)]^+$ model complex, the Ag^+ ion is bound to the piperazine N5 atom, while in $[Ag–Sil(Pyz)]^+$ the Ag^+ is bound to the pyrazole N3 atom. Because individual atom numbering was required for the computational analysis, the sildenafil atom numbering scheme was adapted accordingly (Scheme 1).

DFT calculations were carried out using Gaussian 16 [47] on the B3LYP/LANL2DZ [48–50] level of theory. The B3LYP functional was selected because it provides a reliable balance between computational cost and accuracy for organic and organometallic systems, while the LANL2DZ basis set and effective core potential are commonly applied for transition-metal-containing complexes, including silver coordination compounds. Solvent effects were not explicitly included in the present calculations; therefore, the optimized structures represent gas-phase approximations intended primarily for comparative structural and electronic analysis of the proposed Ag–sildenafil coordination modes.

The docking studies were performed using the Molecular Operating Environment (MOE) platform, Version 2019.01 (Chemical Computing Group ULC, Montreal, QC, Canada) [51]. The initial scoring function setting was London dG, followed by GBVI/WSA dG for final scoring. The docking refinement employed a forcefield-based protocol to improve pose accuracy. A directed docking approach was used, where the binding sites were predefined based on key active-site residues for the target receptor. The receptor structures were retrieved from the Protein Data Bank (PDB). The human M2 muscarinic acetylcholine receptor was obtained from PDB ID 3UON [52] and the human α3β4 nicotinic acetylcholine receptor was obtained from PDB ID 6CNJ [53]. Prior to docking, receptor structures were prepared by removal of crystallographic water molecules and co-crystallized ligands, followed by protonation and energy minimization within MOE. To validate the docking workflow, the co-crystallized ligands associated with the receptor structures were re-docked into their corresponding binding sites, yielding structures consistent with the reported experimental binding orientations. Minimum energy structures were obtained using the "Energy Minimize" option in the MOE platform, which employs the MMFF94x force field. The optimized structural parameters, including selected bond lengths, bond angles, and dihedral angles for the $[Ag–Sil(Pip)]^+$ and $[Ag–Sil(Pyz)]^+$ models, are summarized in Tables S4 and S5 (Supplementary Materials) and compared with the corresponding experimental crystallographic data of sildenafil citrate monohydrate (QEKVIM).

2.6. Clinical Study

The experimental details of the clinical study, including study design, inclusion and exclusion criteria, outcome definitions, and the CONSORT flow diagram, are provided in the Supplementary Materials. In brief, 91 participants diagnosed with acute anal fissures were assessed and randomized into two groups: Participants were allocated using a simple

randomization procedure with an approximate 1:2 allocation ratio (intervention:control). The study was conducted in a blinded manner, where patients and outcome assessors were unaware of group assignment. The intervention group received the Ag@Sil NP ointment (n = 31), while the control group received a placebo ointment (n = 60). The placebo formulation contained the same ointment base and excipients as the active formulation, but without Ag@Sil NPs. During the study, 16 participants withdrew (6 intervention; 10 control) due to lack of clinical improvement, non-adherence to treatment, or loss to follow-up, resulting in 25 participants in the intervention group and 50 participants in the control group that completed the study and were included in the final per-protocol analysis.

Clinical outcomes included fissure healing as the primary endpoint, while secondary outcomes included pain during defecation and at rest, rectal bleeding, itching, and sensation of mass in the anal area. Clinical assessments were performed using physical examination and patient questionnaires after the completion of the two-week treatment period. Patients were additionally monitored for local or systemic adverse effects throughout the study.

The primary information needed to calculate the sample size was obtained from previous studies [54,55]. The sample size was calculated with 95% confidence and 80% power, considering the changes in the pain variable within two weeks as reported in the mentioned studies. Statistical analyses for sample size estimation and power analysis were performed using G*Power 3 (Version 3.1) [56] for sample size estimation and power analysis. Descriptive and inferential statistics were conducted to evaluate differences between groups and changes over time. Categorical variables, including clinical outcomes such as fissure healing, pain, bleeding, itching, and related symptoms, were analyzed using chi-square and Fisher's exact tests where appropriate. All statistical tests were two-sided, and a p-value < 0.05 was considered as statistically significant. The analysis was performed on a per-protocol basis, including only participants who completed the study. Clinical outcome analyses were conducted on a per-protocol basis, including only participants who completed the two-week treatment and post-treatment evaluation. It should also be noted that baseline differences between the intervention and control groups, particularly regarding age and some symptom frequencies, may have influenced treatment outcomes and represent a limitation of the present exploratory study.

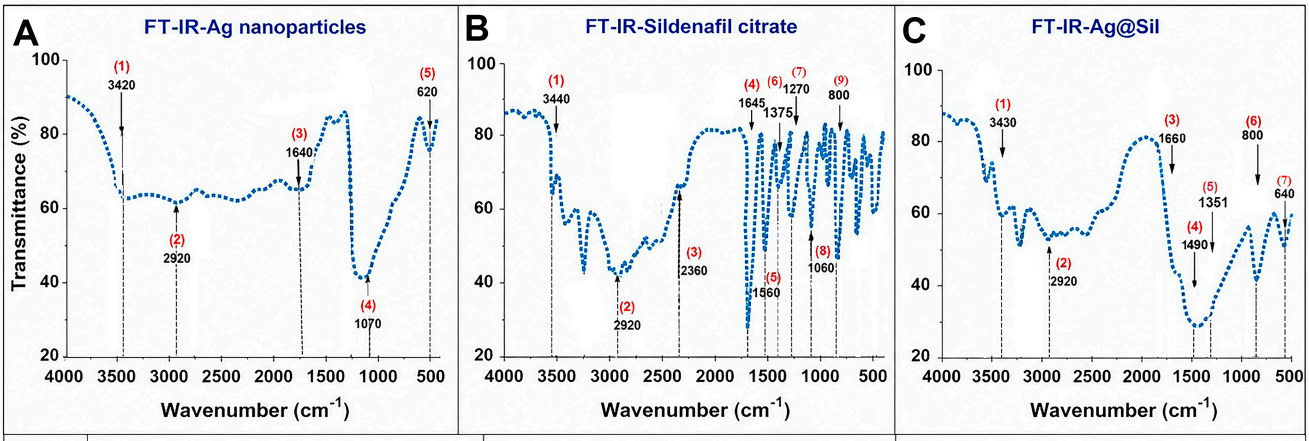
No formal adjustment for multiple comparisons was applied, as this investigation was exploratory in nature and aimed at assessing preliminary efficacy and safety of the Ag@Sil formulation.

3. Results and Discussion

3.1. Synthesis and Characterization of the Ag@Sil NPs

The sildenafil-modified Ag NPs (Ag@Sil NPs) were prepared by impregnating PVP-coated Ag NPs with sildenafil citrate in DMSO solution. Centrifugation and washing with water and acetone was done to remove loosely bound sildenafil molecules.

The Fourier-transform infrared (FT-IR) spectrum of the PVP-stabilized Ag NPs (Figure 1A) shows the characteristic absorption bands associated with PVP on the Ag surface [57]. A broad band centered at 3420 cm^{-1} is attributed to O–H/N–H stretching vibrations, while the band at 2920 cm^{-1} corresponds to aliphatic C–H stretching vibrations. The characteristic amide-related vibration of PVP appears at around 1640 cm^{-1} and is assigned to the C=O stretching vibration (amide I band). In addition, the absorption band at around 1070 cm^{-1} is attributed to C–O stretching vibrations of the polymer matrix. A weak band at around 620 cm^{-1} can be associated with Ag–O and/or Ag–N interactions between the stabilizing matrix and the NP surface.



Peak No.	A. FT-IR-Ag nanoparticles		B. FT-IR-Sildenafil citrate		C. FT-IR-Ag@Sil	
	Wavenumber (cm^{-1})	Assignment	Wavenumber (cm^{-1})	Assignment	Wavenumber (cm^{-1})	Assignment
(1)	3420	O–H / N–H stretching	3440	O–H / N–H stretching	3430	O–H / N–H stretching
(2)	2920	C–H stretching	2920	C–H stretching	2920	C–H stretching
(3)	1640	C=O (amide I)	2360	N≡C stretching	1660	C=O (amide I)
(4)	1070	C–O stretching	1645	C=O (amide I)	1490	C–N stretching
(5)	620	Ag–O / Ag–N stretching	1560	N–H bending / C=C stretching	1351	S=O stretching
(6)	–	–	1375	S=O stretching	800	Aromatic C–H out-of-plane
(7)	–	–	1270	C–N stretching	640	Ag–O / Ag–N stretching
(8)	–	–	1060	C–O stretching	–	–
(9)	–	–	800	Aromatic C–H out-of-plane	–	–

Figure 1. FT-IR spectra of (**A**) the PVP-stabilized Ag NPs, (**B**) sildenafil citrate, and (**C**) Ag@Sil NPs with characteristic peaks marked (**top**) and assignments (**bottom**).

The FT-IR spectrum of sildenafil citrate (more precisely, the sildenafil–citric acid cocrystal) (Figure 1B) exhibits several characteristic vibrational features [43,44,58]. The broad absorption band around 3440 cm^{-1} corresponds to O–H/N–H stretching vibrations originating from hydroxyl and secondary amine groups. The absorption band around 2920 cm^{-1} is assigned to aliphatic C–H stretching vibrations. A weak band observed at 2360 cm^{-1} is attributed to N≡C stretching vibrations. The strong absorption band at 1645 cm^{-1} corresponds to C=O stretching vibrations, while the band at around 1560 cm^{-1} is assigned to N–H bending together with aromatic C=C/C=N stretching modes. The prominent sulfonyl S=O stretching vibration appears at 1375 cm^{-1}. Additional characteristic absorptions include the C–N stretching vibration at 1270 cm^{-1}, the C–O stretching band at around 1060 cm^{-1}, and the aromatic C–H out-of-plane vibration at around 800 cm^{-1}.

In the FT-IR spectrum of Ag@Sil (Figure 1C), the characteristic sildenafil-related bands are retained, confirming the successful incorporation of sildenafil onto the NP surface. The Ag@Sil spectrum shows absorption bands at 3430 cm^{-1} (O–H/N–H stretching), 2920 cm^{-1} (C–H stretching), and 1660 cm^{-1} corresponding to carbonyl/amide-related vibrations. Additional characteristic bands are observed at 1490 cm^{-1} (C–N stretching), 1351 cm^{-1} (S=O stretching), and around 800 cm^{-1} assigned to aromatic C–H out-of-plane vibrations. Compared with pure sildenafil citrate, several characteristic bands exhibit slight shifts and broadening, particularly the vibrations related to the C=O, S=O, and C–N functionalities, indicating changes in the local electronic environment after interaction with the Ag NP surface. Furthermore, the appearance of the low-frequency band near 640 cm^{-1}, attributed to Ag–O and/or Ag–N interactions, provides additional evidence for coordination between sildenafil functional groups and the Ag surface. Compared with bare Ag NPs, which mainly display broad features originating from the stabilizing PVP matrix, the Ag@Sil spectrum strongly supports the presence of sildenafil with modified vibrational characteristics. Together with the extensive washing procedure applied after synthesis, the

retention of characteristic sildenafil bands combined with systematic peak shifts and the emergence of metal–ligand vibrations strongly support successful surface functionalization through coordination of sildenafil molecules to the Ag NPs, rather than simple physical adsorption or mechanical mixing.

The transmission electron microscopy (TEM) image of Ag@Sil NPs (Figure 2A) reveals predominantly spherical NPs with nanoscale dimensions and relatively uniform morphology. A faint halo surrounding the darker NP cores is attributed to the surface coating by PVP and sildenafil molecules and has similarly been observed in related NP systems [2,4,5,11]. Spherical morphologies are characteristic for Ag NPs synthesized in the lower nm size range [2,4,5].

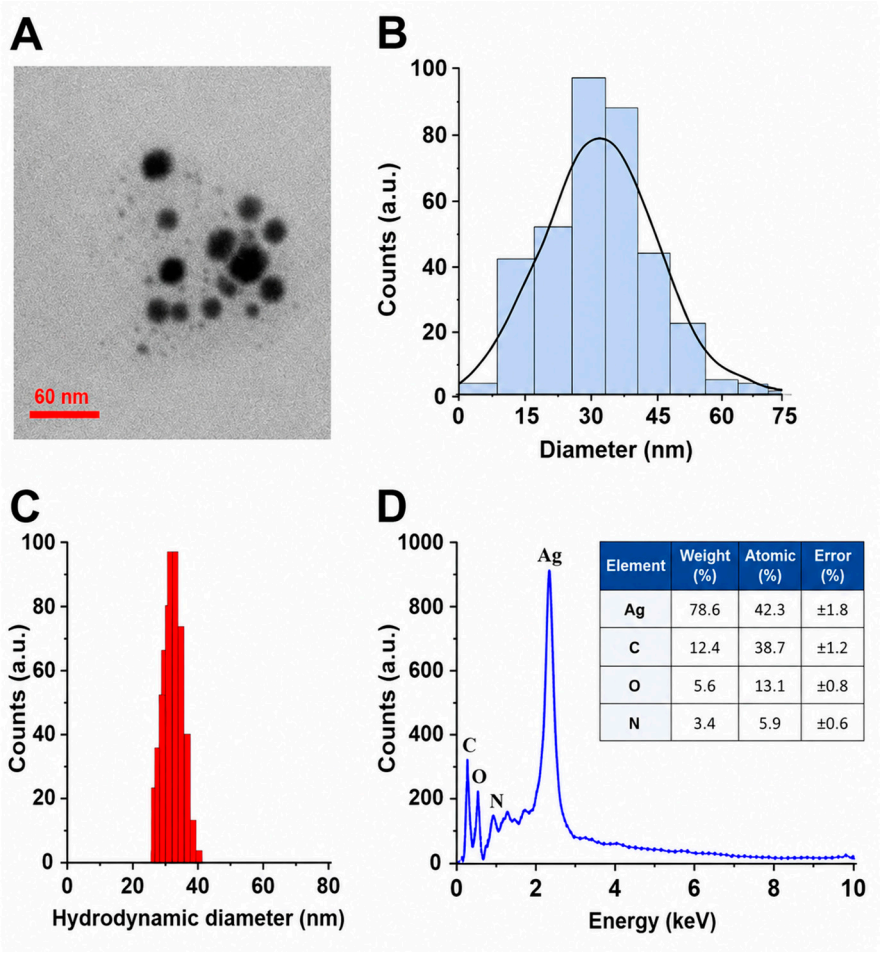


Figure 2. (**A**) Transmission electron microscopy (TEM) image of Ag@Sil NPs recorded at an accelerating voltage of 200 kV with a magnification of about ×200,000. (**B**) Particle size distribution histogram from TEM analysis based on >100 NPs. The average particle diameter was determined to 25 ± 8 nm (mean ± SD). (**C**) DLS size distribution of Ag@Sil NPs with an averaged hydrodynamic diameter of 29 ± 4 nm and a polydispersity index (PDI) of 0.21. (**D**) EDX analysis of the Ag@Sil NPs confirming the presence of Ag together with C, N, and O originating from the PVP/sildenafil surface coating.

To obtain a more quantitative evaluation of the particle size distribution, the diameters of more than 100 NPs were determined from TEM images, with the resulting histogram shown in Figure 2B. The particle size distribution follows an approximately Gaussian profile with an average particle diameter of 25 ± 8 nm, with most particles distributed within the 15–45 nm range. Only a small fraction of larger particles above 50 nm was observed, indicating a relatively narrow size distribution and moderate polydispersity of the synthesized NPs.

The dynamic light scattering (DLS) measurements (Figure 2C) further confirmed the nanoscale dimensions of the Ag@Sil NPs and were in good agreement with the TEM-derived particle size distribution. The DLS analysis showed a hydrodynamic diameter centered at 29 ± 4 nm with a polydispersity index (PDI) of 0.21, indicating a relatively narrow size distribution and good colloidal homogeneity. The slightly larger hydrodynamic diameter observed by DLS compared with TEM can be attributed to the contribution of the solvation layer together with the PVP/sildenafil coating surrounding the metallic Ag core.

The EDX elemental analysis (Figure 2D) confirmed Ag as the dominant element in the Ag@Sil NPs, together with smaller amounts of C, O, and N originating from the PVP/sildenafil surface coating. The observed elemental composition agrees with previous reports on structurally related functionalized Ag NP systems [2,6,10,11].

The powder XRD patterns (Figure 3A) of both PVP-stabilized Ag NPs and sildenafil-modified Ag NPs (Ag@Sil) display identical characteristic diffraction peaks at 2θ = 38.18°, 44.25°, 64.72°, and 77.40°, which can be indexed to the (111), (200), (220), and (311) planes of face-centered cubic (fcc) Ag. The absence of additional peaks indicates that no secondary phases, such as silver oxide or other impurities, are present. Importantly, no noticeable shift or broadening of the diffraction peaks is observed after surface modification with sildenafil, confirming that the crystalline structure of the Ag NPs remains unchanged.

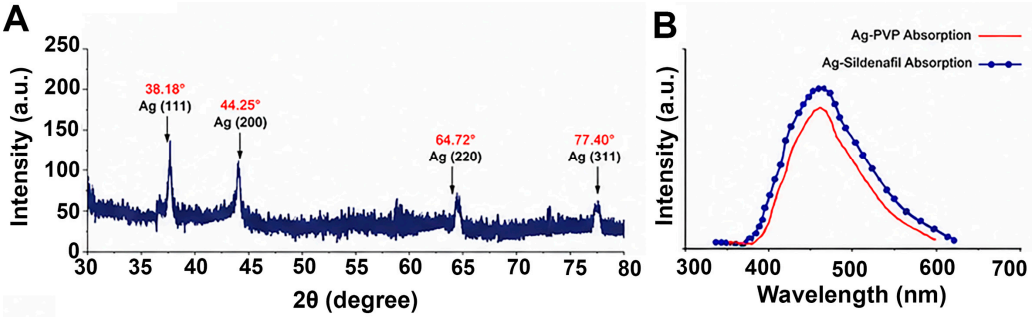


Figure 3. (**A**) Powder X-ray diffraction (XRD) patterns and (**B**) UV–Vis absorption spectra of Ag NPs stabilized with PVP and Ag@Sil NPs.

Similarly, the UV–Vis absorption spectra (Figure 3B) show a strong surface Plasmon resonance (SPR) band centered around 400–600 nm for both samples, which is characteristic of spherical Ag NPs in the nanoscale range. The position and shape of the SPR band remain essentially unchanged upon modification with sildenafil, indicating that the particle size distribution and optical properties are not significantly affected by the surface functionalization.

Overall, the XRD and UV–Vis results consistently demonstrate that the modification of Ag NPs with sildenafil does not alter the intrinsic structural or optical properties of the metallic core, but rather involves surface-level interactions.

3.2. Preliminary Clinical Evaluation of Ag@Sil Ointment

Given the considerable burden of acute anal fissure on patient quality of life, and the limitations associated with existing treatments, such as the risk of fecal incontinence from surgery [19,20,59,60], the high costs and invasiveness of botulinum toxin injections [19,21–23], and the side effects of topical agents like diltiazem or nitrates [19,61,62], we carried out a clinical study using an Ag@Sil NP-containing ointment (0.1 wt%) for the treatment of anal fissures (experimental details are provided in the Supplementary Materials). A total of 25 participants in the intervention group and 50 participants in the control group completed the full two-week treatment course and post-treatment evaluation. Table S1 summarizes the demographic data of the study participants. The mean age in the intervention group

was 40.9 years (range: 18–75 years), while in the control group it was 55.5 years (range: 29–84 years). Female participants represented the majority in both groups, comprising 73% of the intervention group and 66% of the control group.

Pre-treatment assessment showed comparable baseline frequencies for most symptoms between both groups (Table S2). Statistically significant differences at baseline were observed for anal pain at rest ($p = 0.05$) and rectal bleeding during examination ($p = 0.001$), with higher severity noted in the intervention group. The primary and key secondary clinical outcomes are summarized quantitatively in Table 1. After two weeks of treatment, the Ag@Sil group showed significantly improved fissure healing rates (84% vs. 38% in the control group, $p = 0.0006$), together with marked reductions in pain at rest, pain during defecation, and rectal bleeding compared with the placebo group.

Table 1. Primary and key secondary clinical outcomes at baseline and after 2 weeks of treatment.

Outcome	Group	n	Baseline (%)	2 Weeks (%)	Absolute Change (%)	*p*-Value [a]
fissure healing	Ag@Sil	25	0	84	+84	0.0006
	Control	50	0	38	+38	
pain at rest	Ag@Sil	25	100	24	−76	0.003
	Control	50	100	62	−38	
pain during defecation	Ag@Sil	25	100	16	−84	0.001
	Control	50	100	54	−46	
rectal bleeding	Ag@Sil	25	100	8	−92	<0.001
	Control	50	100	46	−54	

[a] *p*-values were calculated using chi-square (two-proportion) tests comparing intervention and control groups at Week 2.

Post-treatment outcomes (Table S3) further showed a marked improvement in anal fissure symptoms among treated participants. More specifically, itching decreased in the intervention group from 58% to 4% (Figure S1), while remaining essentially unchanged in the control group (56% before and after treatment). Similarly, rectal bleeding was reduced from 77% to 12% in the intervention group, compared with only a minor reduction in the control group (76% to 72%) (Figure S2). Pain during rest and pain after defecation also showed substantial improvement in the intervention group. Pain during rest dropped from 54% to 12%, and pain after defecation from 85% to 26% (Figures S3 and S4). In contrast, the control group showed no notable improvements in these symptoms. Additionally, the sensations of pulsation and the presence of a mass improved significantly in the intervention group (38% to 4%), with no meaningful changes in the control group (Figure S5). Clinical examination findings supported these symptomatic results. Bleeding during examination decreased from 27% to 4% in the intervention group (Figure S6), while it increased slightly in the control group (66% to 70%). Pain during examination was also significantly reduced in the intervention group from 73% to 15% (Figure S7), while remaining essentially unchanged in the control group at 82%.

Although our clinical study remained preliminary in character, the Ag@Sil NP formulation showed promising therapeutic potential by significantly reducing pain during defecation, resting anal pain, rectal bleeding, and other associated symptoms, while also promoting fissure healing within the intervention group. Throughout the two-week treatment period, no adverse effects or local reactions were reported in either the intervention or control groups. The treatment was well tolerated, and no systemic or dermatologic complications associated with the study formulation were observed. The marked differences observed between the intervention and placebo groups suggest that the therapeutic effects are likely associated with the Ag@Sil NP formulation, although

larger controlled clinical studies will be necessary to fully exclude placebo-related and confounding effects.

Conventional treatment options for acute anal fissure include topical nitrates, calcium-channel blockers such as diltiazem or nifedipine, botulinum toxin injections, and surgical intervention [19–23,59–62]. Although these approaches may improve fissure healing and symptom control, they are frequently associated with adverse effects such as headache, hypotension, procedural discomfort, recurrence, or the risk of fecal incontinence following surgical treatment. In the present study, the Ag@Sil NP-containing ointment showed marked reductions in pain, rectal bleeding, and fissure-related symptoms within a short treatment period, without observable local or systemic adverse effects. While the present clinical investigation remains preliminary in nature and involves a limited sample size, the observed therapeutic response compares favorably with previously reported outcomes for several conventional topical treatment strategies.

NP-based therapeutic systems have attracted increasing interest in wound healing and mucosal repair because they can combine antimicrobial activity with controlled drug delivery and local pharmacological action. Ag NPs are known for their broad-spectrum antimicrobial and anti-inflammatory properties and have been widely investigated in tissue repair applications. Functionalization of Ag NPs with biologically active ligands has been proposed as an effective strategy to achieve multifunctional therapeutic systems with synergistic activity [1–3,6–12]. In the present study, the Ag@Sil NPs may provide combined therapeutic benefits through the antimicrobial and wound-healing properties of Ag NPs together with the vasodilatory and smooth-muscle-relaxing effects of sildenafil, which may contribute to improved blood flow and accelerated fissure healing.

3.3. Density Functional Theory (DFT) Structure Optimization

There are two anhydrous polymorphic forms, I and II, of pure sildenafil [45]. From most solvents, form I is obtained. Additionally, there are more than 40 structures where sildenafil is co-crystallized with solvents, saccharinates, and various acids, including citric acid as in the commercially available drug [45]. In the Cambridge Crystallographic Database (CCDC), four molecular structures are reported for sildenafil: QEKVEI, CIHFAD, QEKVIM, and RIBVAC.

In order to model Ag-bound sildenafil molecules, we created two model Ag–Sil complexes. In $[Ag–Sil(Pip)]^+$ an Ag^+ ion is binding to the peripheral piperazine N atom, which is N5 in our nomenclature (Figure 4A), while $[Ag–Sil(Pyz)]^+$ features a pyrazole-N-bound Ag^+, at what we called N3 position (Figure 4B). Both $[Ag–Sil]^+$ models were geometry-optimized on the B3LYP/LANL2DZ level of theory (Figure 4). Despite the binding of the Ag^+ ion, the calculated structures (Figure 4, data in Table S4) are both quite similar to the reported structure of the sildenafil citrate monohydrate [44] or the methanol clathrate [46]. Alternative binding points of sildenafil on Ag NPs are provided by the planar oxo-1*H*-pyrazolo-pyrimidine core with the pyrazole N2 atom, the pyrimidinone N4 and N7 atoms, the pyrimidinone O7, but also the amino N6 atom on the piperidine. The sulfonyl group ($–SO_2–$) and the ethoxy function on the central phenyl core, probably fail to coordinate to Ag^+, as the soft Ag^+ prefers soft atom such as N [63]. Alternatively, the planar π system might coordinate to the Ag surface. Furthermore, Van der Waals forces could potentially bind sildenafil molecules on the surface. Our choice fell on the most basic N atoms of the sildenafil system, which are also both sterically favored (not hindered). The two $[Ag–Sil]^+$ models were compared in the docking study.

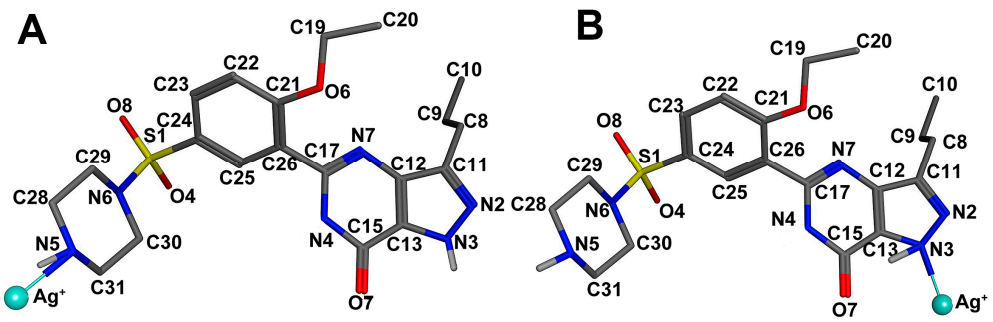


Figure 4. DFT-optimized geometry of the two molecular [Ag–Sil]$^+$ models [Ag–Sil(Pip)]$^+$ (**A**) and [Ag–Sil(Pyz)]$^+$ (**B**) on the B3LYP/LANL2DZ level of theory. The Ag^+ ions are shown as light-green balls. Note that the atom numbering differs to the established numbering shown in Scheme 1 Left.

3.4. Molecular Docking

To evaluate a potential mechanistic pathway for the use of Ag@Sil NPs in the treatment of acute anal fissures, molecular docking simulations were conducted on three ligand systems: the molecule nitroglycerin, and *L*-arginine and the two [Ag–Sil]$^+$ model complexes on the human M2 muscarinic acetylcholine receptor and the human α3β4 nicotinic acetylcholine receptor, with the docking scores and RMSD values summarized in Table 2. The dominant interaction patterns observed in the docking simulations included hydrogen bonding, $\pi\cdots\pi$ interactions, hydrophobic contacts, and electrostatic interactions involving sildenafil functional groups and amino acid residues within the receptor binding sites (Figures 5 and 6).

Table 2. Docking scores and RMSD values [a].

Ligand	Receptor	Docking Score (kcal/mol)	RMSD
L-arginine	M2	−5.32	0.915
L-arginine	α3β4	−8.05	0.910
Nitroglycerin	M2	−8.46	0.861
Nitroglycerin	α3β4	−8.74	0.972
Sildenafil	M2	−10.62	0.728
Sildenafil	α3β4	−9.31	0.925
[Ag–Sil(Pyz)]$^+$	M2	−12.24	0.452
[Ag–Sil(Pip)]$^+$	M2	−10.92	0.634
[Ag–Sil(Pyz)]$^+$	α3β4	−9.62	0.987
[Ag–Sil(Pip)]$^+$	α3β4	−11.21	0.871

[a] Root mean square deviation (RMSD).

For the muscarinic M2 receptor, [Ag–Sil(Pyz)]$^+$ showed the highest affinity with a docking score of −12.24 kcal/mol and excellent pose reliability (RMSD = 0.452). This is even higher than the binding to sildenafil (−10.62 kcal/mol) and higher than the [Ag–Sil(Pip)]$^+$ isomer (−10.92 kcal/mol). For the nicotinic acetylcholine receptor α3β4, binding of [Ag–Sil(Pip)]$^+$ (−11.21 kcal/mol) was slightly higher compared to that of the Pyz derivative (−9.62 kcal/mol) and to sildenafil (−9.31 kcal/mol). Both are outperforming *L*-arginine and nitroglycerine by far.

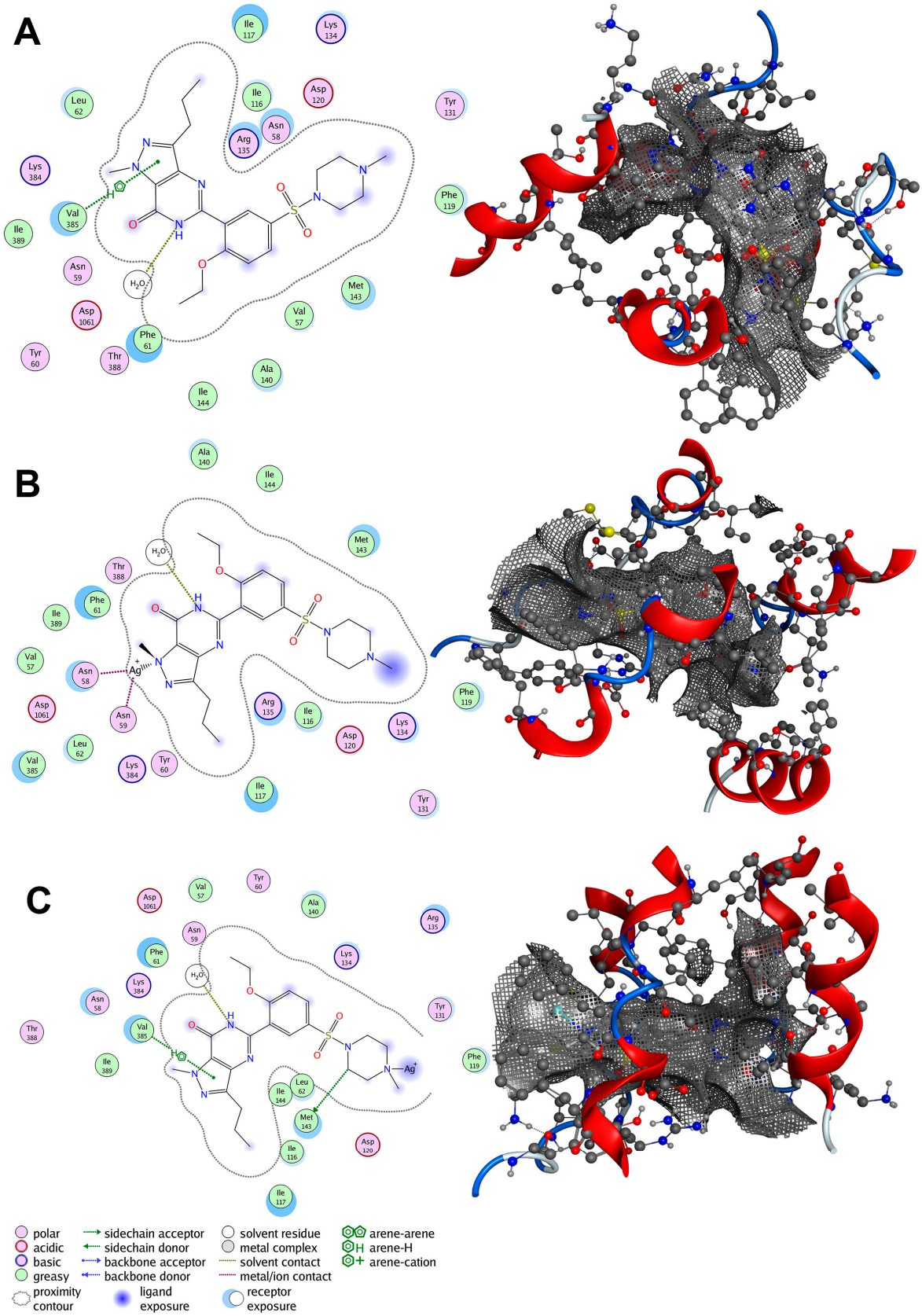


Figure 5. Interaction pattern and surface map of the muscarinic M2 receptor with (**A**) sildenafil, (**B**) [Ag–Sil(Pyz)]$^+$, and (**C**) [Ag–Sil(Pip)]$^+$.

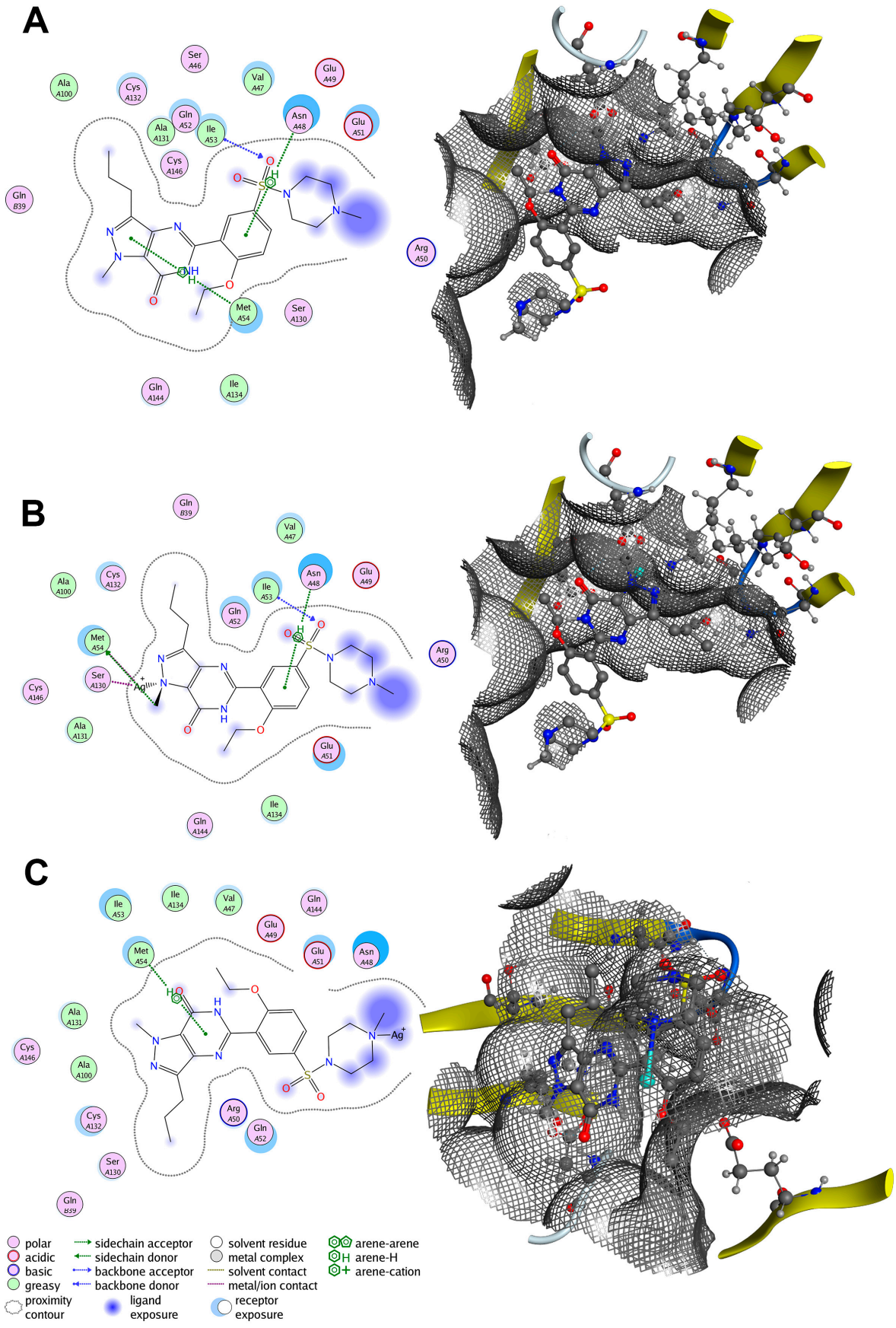


Figure 6. Interaction pattern and surface map of the nicotinic acetylcholine α3β4 receptor with (**A**) sildenafil, (**B**) [Ag–Sil(Pyz)]$^+$, and (**C**) [Ag–Sil(Pip)]$^+$.

For the established muscarinic receptor antagonist abietic acid, a decahydrophenanthrene-1-carboxylic acid, a docking score against the muscarinic M2 receptor of −8.7 kcal/mol was recently reported [64]. The two plant-based M2 antagonist molecules quercetin (3,3′,4′,5,7-pentahydroxyflavone) and hyoscine (1α*H*,5α*H*-tropan-3α-ol,6β,7β-epoxy-(−)-tropate) showed docking scores of −8.2 and −7.5 kcal/mol [65]. A score of −7.3 kcal/mol was reported for the antiemetic nerolidol (3,7,11-trimethyl-1,6,10-dodecatrien-3-ol, a terpene) [66] and an even lower score of −5.36 kcal/mol was very recently reported for 1-(3-(2-chlorophenyl)-4,5-dihydroisoxazol-5-yl) pyrrolidin-2-one [67]. In a comprehensive study, the docking scores of potentially pharmaceutically active components from *Qusqualis indica* (Chinese honeysuckle) with values of −5.63 (coumaric acid), −5.92 (urosolic acid), −6.70 (lupeaol), −7.73 (quercetin), and −7.96 (sisterol) confirm these studies quite well [68]. The markedly higher values for the two $[Ag–Sil]^+$ models and sildenafil of more than −10 kcal/mol suggest a potential for interaction with the investigated targets.

The docking scores of the $[Ag–Sil]^+$ models and sildenafil to the nicotinic acetylcholine receptor α3β4 of around −10 kcal/mol lie in the same range as those found for the four recently reported quinnuclidine–triazole compounds (*R*) or (*S*)-2-(4-(4-(X)-3-fluorophenyl)-1*H*-1,2,3-triazol-1-yl)quinuclidine with X = OH or OBn) (−10 to −14 kcal/mol) [69]. For both desnitro-imidacloprid and the descyano-thiacloprid-olefin, two neonicotine metabolites, suspected as highly selective α3β4 antagonist, radioligand binding assays gave binding energies of about −36 kcal/mol [70]. For the docking of GAT2802 (*R*-1-(3,5-diisopropyl-1*H*-pyrazol-1-yl)-3-methylbutan-2-yl (4-ethoxyphenyl)carbamate) to the α4β2 variant, values of around −12 to −17 kcal/mol for were reported making GAT2902, together with a positive allosteric modulation, a lead compound for the development of nicotinic acetylcholine receptor (nAChR) positive allosteric modulator (PAM) [71]. The docking score for nicotine at the α4β2 receptor was reported to be −41.45 kcal/mol [72]. Thus, the docking scores of the $[Ag–Sil]^+$ models and sildenafil to the nicotinic acetylcholine receptor α3β4 suggest only moderate binding when compared to the other examples.

The residue analysis for the interaction of sildenafil with the muscarinic M2 receptor showed dominating apolar (hydrophobic) interactions with Val385Leu62, Ile117, Ile116, Phe119, Met243, Val57, Ala140, Ile144, and Phe62 and polar (hydrophilic) interactions with Asp1061, Asn50, Lys384, Arg135, Asn58, Asp120, and Tyr131, among others (Figure 5A). Polar, hydrophilic···hydrophilic interactions are hydrogen bonds between the amine or carbonyl groups of the ligands and polar amino acid residues, such as Asp, Asn, Arg, and Lys. An interesting hydrophilic feature is a water molecule closed to the pyrimidinone N4–H and Asp1061 and Asn59. An interesting apolar, hydrophobic···hydrophobic interaction is the C–H···π stacking of Val385 with the pyrazole moiety. Other hydrophobic···hydrophobic interactions are Van der Waals type apolar C–H···X interactions, which are dominant along the piperidinyl–sulfonyl-phenyl-O-ethyl moiety.

Overall, the situation is not very different for $[Ag–Sil(Pyz)]^+$ where both polar, hydrophilic and apolar hydrophobic interactions with the receptor are found (Figure 5B). As expected the coordinating Ag^+ on the pyrazole renders this part highly polar and replaces the hydrophobic C–H···π stacking of the pyrazole. The general picture for the $[Ag–Sil(Pip)]^+$ model complex is similar to that of the Pyz derivative with mixed hydrophilic/hydrophobic interactions (Figure 5C). Markedly different is the change in polarization of the outer part of the piperidinyl–sulfonyl-phenyl-O-ethyl moiety from dominating hydrophobic interactions for sildenafil and the Pyz complex to rather hydrophilic interactions for the Pip derivative, while a quite hydrophobic pocket is formed in which the apolar Met143, Leu62, Ile144, Ile116, and Ile17 are interacting with the piperidine C–H, the pyrimidinone N7, and the propyl C–H function. This is obviously caused by the Ag^+

coordination. All three ligands are well-embedded in the M2 receptor with only small parts exposed.

Nitroglycerin and arginine are engaged with markedly fewer residues and lacked deeper hydrophobic or hydrophilic contacts (Figure S8), which is in line with the lower docking scores (Table 2). Both ligands are well-embedded in the M2 receptor.

The reported docking of scopolamine to M2 involved mainly Ala194 and Trp155 with binding to the π system of the phenyl ring, Asn404 binding with the ester C=O, and Tyr426, Trp409, Tyr403, and Cys429 interacting with the central tertiary amine of scopolamine [64]. The carboxylic group of abietic acid interacts mainly with Tyr83 and Asn419, while Trp422 and Tyr426 show hydrophobic···hydrophobic interactions with the polyhydrophenanthrene moiety [64]. In an earlier study, quercetin was found to interact with the Phe181 and Tyr104 residues, as well as with Trp422, while scopolamine shows a main interaction with Tyr179 [65]. For nerolidol a plethora of interactions with M2 was reported, including hydrogen bonding with Ser107 and hydrophobic···hydrophobic interactions with Ala194, Val111, Trp155, Tyr403, Tyr104, Tyr426, and Trp40, to name only interactions shorter than 4 Å [66]. Overall, the docking interactions of our ligands are quite dissimilar to the above discussed, which is not unexpected in view of the very different structures.

With the nicotinic acetylcholine α3β4 receptor, sildenafil showed important polar contacts of the piperidinyl–sulfonyl group to CysA146, GlnA52, AsnA48, GluA49, GluA51, and ArgA50 (Figure 6A). Hydrophobic C–H···π stacking of the pyrazole with MetA54 is complemented by a similar interaction of the central phenyl with AsnA48. The situation is only slightly different for $[Ag–Sil(Pyz)]^+$ which maintains both polar and apolar interactions (Figure 6B). While the pyrazole moiety has gained in polarity through the Ag^+-coordination with a strong SerA130···Ag^+ polar interaction, the other part of the molecule remains rather unchanged compared to sildenafil, which includes the C–H···π stacking of the central phenyl with AsnA48. For the $[Ag–Sil(Pip)]^+$ complex, the coordination of Ag^+ rendered the entire piperidyl-sulfonyl-phenyl-O-ethyl unit quite polar with dominating hydrophilic interactions to the receptor (Figure 6C). Overall, all three ligands are reasonably embedded within the receptor, with the exception of the piperidine moiety, which is not altered through Ag^+ coordination.

Very different binding is found when comparing *L*-alanine and nitroglycerin (Figure S9). Both maintain quite mixed hydrophobic/hydrophilic contacts with the receptor. Overall, compared with the three ligands sildenafil, $[Ag–Sil(Pyz)]^+$ and $[Ag–Sil(Pip)]^+$ the number of interactions is markedly reduced, which is in line with the lower docking scores (Table 2).

The above discussed descyano-thiacloprid-olefin, suspected to be a potent α3β4 antagonist, interacts essentially with the Tyr93, Trp149, Tyr197 residues from the so-called aromatic box, and with Trp59 [70]. The four previously studied quinnuclidine–triazole compounds showed hydrogen bonding to the Asp173 residue, some of them additionally to Ser148 [69]. Additionally, cation···π (Asp173), hydrophobic···hydrophobic π···π (Trp59, Trp149, Tyr190, Tyr197), and halogen bond interactions (Trp149) were reported [69]. As stated already for the docking to the M2 receptor, the docking interactions of our ligands to α3β4 are quite dissimilar to those discussed above.

4. Conclusions

This study reports the synthesis, characterization, and preliminary clinical evaluation of a novel topical formulation based on sildenafil-modified silver nanoparticles (Ag@Sil NPs) for the treatment of acute anal fissures. The Ag@Sil system was successfully prepared via surface functionalization of PVP-stabilized Ag NPs, characterized using Transmission electron microscopy (TEM), dynamic light scattering (DLS), energy-dispersive X-ray (EDX)

spectroscopy, and Fourier-transform infrared (FT-IR) spectra, and incorporated into a topical ointment. In a randomized preliminary clinical study, application of the formulation led to improvements in key symptoms, including pain at rest and during defecation, rectal bleeding, itching, pulsation sensation, and mass feeling over a two-week treatment period. No adverse effects were reported, suggesting a favorable short-term safety profile.

Molecular docking studies targeting the muscarinic M2 and nicotinic α3β4 acetylcholine receptors indicated that the proposed $[Ag–Sil]^+$ models with Ag^+ coordinated to either piperazine-N or pyrazole-N sites, exhibit slightly stronger binding affinities compared to sildenafil alone, and notably higher docking scores than *L*-arginine and nitroglycerin. While residue-level interaction analysis revealed only subtle differences between sildenafil and its Ag^+ complexes, more pronounced differences were observed relative to the reference compounds, consistent with the calculated binding energies. These findings suggest that the incorporation of Ag^+ does not diminish, and may modestly enhance, the interaction potential of sildenafil with cholinergic receptors.

However, the docking results should be regarded as exploratory and supportive rather than definitive evidence of mechanisms. Likewise, the clinical findings are preliminary and limited by sample size and baseline imbalances between groups. Therefore, while the combined antimicrobial and pharmacological properties of Ag@Sil NPs indicate potential as a multifunctional topical therapeutic system, further well-powered, rigorously controlled clinical trials and mechanistic studies are required to confirm efficacy, safety, and mode of action.

Supplementary Materials: The following supporting information can be downloaded at: https://www.mdpi.com/article/10.3390/applnano7020017/s1, The Supplementary Materials file contains evaluation plots of the clinical study, tables with demographic data of the study participants and prevalence of signs and symptoms, as well as DFT-calculated metrics for the two $[Ag–Sil]^+$ models: **1. Materials**; **2. Clinical Study**; **3. Docking Study**; **Supporting Figures**: Figure S1: Diagram comparing itching before/after treatment for control and treatment group. Figure S2: Diagram comparing anal bleeding before/after treatment for control and treatment group. Figure S3: Diagram comparing anal pain during rest before/after treatment for control and treatment group. Figure S4: Diagram comparing anal pain after defecation before/after treatment for control and treatment groups. Figure S5: Diagram comparing feeling pulse after defecation before/after treatment for control and treatment group. Figure S6: Diagram comparing bleeding during examination before/after treatment for treatment and control group. Figure S7: Diagram comparing pain during examination before/after treatment for treatment and control group. Figure S8: Interaction pattern and surface map of the muscarinic M2 receptor with A) *L*-arginine and B) nitroglycerin. Figure S9: Interaction patterns and surfaces map of the nicotinic acetylcholine α3β4 receptor with A) *L*-arginine and B) nitroglycerin. **Supporting Tables**: Table S1: The demographic data of the study participants. Table S2: Prevalence of signs and symptoms of anal fissure in participants before treatment. Table S3: Prevalence of signs and symptoms of anal fissure in participants post-treatment. Table S4: Selected DFT-calculated metrics of the $[Ag–Sil(Pip)]^+$ model and the experimental structure sildenafil citrate monohydrate. Table S5: Selected DFT-calculated metrics of the $[Ag–Sil(Pyz)]^+$ model and the experimental structure of sildenafil citrate monohydrate.

Author Contributions: M.D. (Mahboubeh Dolatyari): investigation, formal analysis, data curation, resources, methodology, and writing—original draft. P.R., M.H., M.K. and M.D. (Mahdi Dolatyari): investigation, methodology, formal analysis, and data curation. H.M.: investigation, software, methodology, formal analysis, data curation, approval. A.R.: conceptualization, resources, methodology, funding acquisition, supervision, and writing—original draft. A.K.: methodology, supervision, writing—original draft, and writing—review and editing. All authors have read and agreed to the published version of the manuscript.

Funding: This research received no external funding.

Institutional Review Board Statement: The study was conducted in accordance with the Declaration of Helsinki. The test protocol was approved by the Tabriz University of Medical Sciences, University Ethics Committee on 12 April 2021 with the approval number IR.TBZMED.REC.1400.045. The IRCT code for the study is IRCT20190701044062N10.

Informed Consent Statement: Informed consent for participation was obtained from all subjects involved in the study.

Data Availability Statement: A CONSORT 2025 checklist is provided detailing where information on the randomized trial is available. Data that is not included in the manuscript or the Supplementary Materials will be made available on request.

Acknowledgments: The authors acknowledge the ASEPE company for support. The graphical abstract was generated with the help of ChatGPT (GPT-5, OpenAI) with its integrated AI-based image generation tool. The originally generated figure was subsequently manually modified by the authors to ensure scientific accuracy, clarity, and originality. No part of the figures is thus subject to copyright issues. The authors have reviewed and edited the output and take full responsibility for the content of this publication.

Conflicts of Interest: Author Mahboubeh Dolatyari was employed by the ASEPE and the NAREKS companies. The remaining authors declare that the research was conducted in the absence of any commercial or financial relationships that could be construed as a potential conflict of interest. Beyond this, the authors declare no conflict of interests.

References

1. Sati, A.; Mali, S.N.; Ranade, T.N.; Yadav, S.; Pratap, A. Silver Nanoparticles (AgNPs) as a Double-Edged Sword: Synthesis, Factors Affecting, Mechanisms of Toxicity and Anticancer Potentials—An Updated Review till March 2025. *Biol. Trace Elem. Res.* **2025**, *204*, 401–452. [CrossRef] [PubMed]
2. Sati, A.; Ranade, T.N.; Mali, S.N.; Yasin, H.K.A.; Samdani, N.; Satpute, N.N.; Yadav, S.; Pratap, A.P. Silver Nanoparticles (AgNPs) as Potential Antiviral Agents: Synthesis, Biophysical Properties, Safety, Challenges and Future Directions–Update Review. *Molecules* **2025**, *30*, 2004. [CrossRef] [PubMed]
3. Almatroudi, A. Unlocking the Potential of Silver Nanoparticles: From Synthesis to Versatile Bio-Applications. *Pharmaceutics* **2024**, *16*, 1232. [CrossRef] [PubMed]
4. De Gusmão, A.B.; De Albuquerque, P.B.S.; De Carvalho Correia, A.C. Use of Metallic Nanoparticles Synthesized from Plant Extracts in Wound Healing—A Review. *Appl. Nano* **2024**, *5*, 205–226. [CrossRef]
5. Dhaka, A.; Mali, S.C.; Sharma, S.; Trivedi, R. A review on biological synthesis of silver nanoparticles and their potential applications. *Res. Chem.* **2023**, *6*, 101108. [CrossRef]
6. Ravine, T.; Yuan, Q.; Howell, M. Biogenic Silver Nanoparticles Processed Twice Using 8M Urea Exhibit Superior Antibacterial and Antifungal Activity to Commercial Chemically Synthesized Counterparts. *Appl. Nano* **2022**, *3*, 187–201. [CrossRef]
7. Dolatyari, M.; Rostami, A. Strong anti-viral nano biocide based on Ag/ZnO modified by amodiaquine as an antibacterial and antiviral composite. *Sci. Rep.* **2022**, *12*, 19934. [CrossRef] [PubMed]
8. Nicolae-Maranciuc, A.; Chicea, D.; Chicea, L.M. Ag Nanoparticles for Biomedical Applications—Synthesis and Characterization—A Review. *Int. J. Mol. Sci.* **2022**, *23*, 5778. [CrossRef] [PubMed]
9. Naganthran, A.; Verasoundarapandian, G.; Khalid, F.E.; Masarudin, M.J.; Zulkharnain, A.; Nawawi, N.M.; Karim, M.; Che Abdullah, C.A.; Ahmad, S.A. Synthesis, Characterization and Biomedical Application of Silver Nanoparticles. *Materials* **2022**, *15*, 427. [CrossRef] [PubMed]
10. Ahire, J.H.; Wang, Q.; Tao, Y.; Chao, Y.; Bao, Y. Amine-Terminated Silver Nanoparticles Exhibit Potential for Selective Targeting of Triple-Negative Breast Cancer. *Appl. Nano* **2024**, *5*, 227–244. [CrossRef]
11. Velgosova, O.; Macák, L.; Lisnichuk, M.; Varga, P. Influence of pH and Temperature on the Synthesis and Stability of Biologically Synthesized AgNPs. *Appl. Nano* **2025**, *6*, 22. [CrossRef]
12. Devi, L.; Kushwaha, P.; Ansari, T.M.; Kumar, A.; Rao, A. Recent Trends in Biologically Synthesized Metal Nanoparticles and their Biomedical Applications: A Review. *Biol. Trace Elem. Res.* **2024**, *202*, 3383–3399. [CrossRef] [PubMed]
13. Veg, E.; Hashmi, K.; Raza, S.; Joshi, S.; Khan, A.R.; Khan, T. The Role of Nanomaterials in Diagnosis and Targeted Drug Delivery. *Chem. Biodivers.* **2025**, *22*, e202401581. [CrossRef] [PubMed]
14. Li, X.; Lin, Y.; Yang, Z.; Guan, L.; Wang, Z.; Liu, A.; Yang, B.; Tang, L.; Lin, Q. Cancer cell membrane biomimetic nanosystem for homologous targeted dual-mode imaging and combined therapy. *J. Colloid Interface Sci.* **2023**, *652*, 770–779. [CrossRef] [PubMed]

15. Gautam, M.; Poudel, K.; Yong, C.S.; Kim, J.O. Prussian blue nanoparticles: Synthesis, surface modification, and application in cancer treatment. *Int. J. Pharm.* **2018**, *549*, 31–49. [CrossRef] [PubMed]
16. Zhang, Y.; Ge, G.; Xu, X.; Wu, J. Ensemble-based virtual screening led to the discovery of novel lead molecules as potential NMBAs. *Molecules* **2024**, *29*, 1955. [CrossRef] [PubMed]
17. Salati, S.A. Anal Fissure an extensive update. *Pol. J. Surg.* **2021**, *93*, 46–56. [CrossRef] [PubMed]
18. Ruymbeke, H.; Geldof, J.; De Looze, D.; Denis, M.A.; De Schepper, H.; Dewint, P.; Gijsen, I.; Surmont, M.; Wyndaele, J.; Roelandt, P. Secondary anal fissures: A pain in the a**. *Acta Gastro-Enterol. Belg.* **2023**, *86*, 58–66. [CrossRef] [PubMed]
19. Lyle, V.; Young, C.J. Anal fissures: An update on treatment options. *Aust. J. Gen. Pract.* **2024**, *53*, 33–35. [CrossRef] [PubMed]
20. Nelson, R.L.; Manuel, D.; Gumienny, C.; Spencer, B.; Patel, K.; Schmitt, K.; Castillo, D.; Bravo, A.; Yeboah-Sampong, A. A systematic review and meta-analysis of the treatment of anal fissure. *Tech. Coloproctol.* **2017**, *21*, 605–625. [CrossRef] [PubMed]
21. De Robles, M.S.; Young, C.J. Real-world outcomes of lateral internal sphincterotomy vs botulinum toxin for the management of chronic anal fissures. *Asian J. Surg.* **2022**, *45*, 184–188. [CrossRef] [PubMed]
22. Herreros, B.; Espi, A.; Rodriguez, C.M.; Granero, E.G.; Sanchiz, V.; Ferriols, F.L.; Almela, P.; Hernandez, V.; Mora, F.; Mínguez, M. Botulinum toxin injection plus topical diltiazem for chronic anal fissure: A randomized double-blind clinical trial and long-term outcome. *Dis. Colon Rectum* **2021**, *64*, 1521–1530. [CrossRef] [PubMed]
23. Vitoopinyoparb, K.; Insin, P.; Thadanipon, K.; Rattanasiri, S.; Attia, J.; McKay, G.; Thakkinstian, A. Comparison of doses and injection sites of botulinum toxin for chronic anal fissure: A systematic review and network meta-analysis of randomized controlled trials. *Int. J. Surg.* **2022**, *104*, 106798. [CrossRef] [PubMed]
24. ElHady, A.K.; El-Gamil, D.S.; Abdel-Halim, M.; Abadi, A.H. Advancements in Phosphodiesterase 5 Inhibitors: Unveiling Present and Future Perspectives. *Pharmaceuticals* **2023**, *16*, 1266. [CrossRef] [PubMed]
25. Kaltsas, A.; Dimitriadis, F.; Zachariou, A.; Sofikitis, N.; Chrisofos, M. Phosphodiesterase Type 5 Inhibitors in Male Reproduction: Molecular Mechanisms and Clinical Implications for Fertility Management. *Cells* **2025**, *14*, 120. [CrossRef] [PubMed]
26. Dunkerly-Eyring, B.; Kass, D.A. Myocardial Phosphodiesterases and Their Role in cGMP Regulation. *J. Cardiovasc. Pharmacol.* **2020**, *75*, 483–493. [CrossRef] [PubMed]
27. Andersson, K.-E. PDE5 inhibitors—Pharmacology and clinical applications 20 years after sildenafil discovery. *Br. J. Pharmacol.* **2018**, *175*, 2554–2565. [CrossRef] [PubMed]
28. Corinaldesi, C.; Di Luigi, L.; Lenzi, A.; Crescioli, C. Phosphodiesterase type 5 inhibitors: Back and forward from cardiac indications. *J. Endocrinol. Investig.* **2016**, *39*, 143–151. [CrossRef]
29. Saikia, Q.; Hazarika, A.; Mishra, R. A Review on the Pharmacological Importance of PDE5 and Its Inhibition to Manage Biomedical Conditions. *J. Pharmacol. Pharmacother.* **2022**, *13*, 246–257. [CrossRef]
30. Zhang, Z.; Huang, W.; Huang, D.; Xu, Z.; Xie, Q.; Tan, X.; He, W.; Yang, W.; Li, G.; Ji, J.; et al. Repurposing of phosphodiesterase-5 inhibitor sildenafil as a therapeutic agent to prevent gastric cancer growth through suppressing c-MYC stability for IL-6 transcription. *Commun. Biol.* **2025**, *8*, 85. [CrossRef] [PubMed]
31. Nemr, M.T.M.; Abdelaziz, M.A.; Teleb, M.; Elmasry, A.E.; Elshaier, Y.A.A.M. An overview on pharmaceutical applications of phosphodiesterase enzyme 5 (PDE5) inhibitors. *Mol. Divers.* **2024**, *29*, 4765–4785. [CrossRef] [PubMed]
32. Pușcașu, C.; Zanfirescu, A.; Negreș, S.; Șeremet, O.C. Exploring the Multifaceted Potential of Sildenafil in Medicine. *Medicina* **2023**, *59*, 2190. [CrossRef] [PubMed]
33. Olarewaju, A.S.; Aliyu, O.M.; Ajani, E.O.; Abdulkareem, Y.F.; Afe, A.; Abdulyakeen, F.O.; Halimat, L.Y.; Sabiu, S.; Singh, K.; Naidoo, K. Mechanisms of *L*-citrulline on phosphodiesterase 5 in erectile dysfunction intervention. *Sci. Afr.* **2025**, *27*, e02572. [CrossRef]
34. Akdogan, N.; Rawat, R.; Ozden, T.; Uzan, F.; Deger, M.; Yılmaz, I.O.; Ates, T.; Arıdogan, I.A. Molecular docking and dynamics simulation analysis of PDE5 inhibitor candidates for erectile dysfunction treatment. *Eur. Rev. Med. Pharmacol. Sci.* **2024**, *28*, 4420–4430. [CrossRef] [PubMed]
35. Zong, T.; Huang, X.; Zhou, W.; Hu, Z.; Jin, L.; Zhan, P.; Zhao, Y.; Sun, J.; Li, G. Advances in the development of phosphodiesterase 5 inhibitors. *Eur. J. Med. Chem.* **2025**, *287*, 117365. [CrossRef] [PubMed]
36. Toque, H.A.; Caldwell, R.W. New approaches to the design and discovery of therapies to prevent erectile dysfunction. *Expert. Opin. Drug Discov.* **2014**, *9*, 1447–1469. [CrossRef] [PubMed]
37. Palanichamy, C.; Pavadai, P.; Panneerselvam, T.; Arunachalam, S.; Babkiewicz, E.; Pandian, S.R.K.; Jeyarajaguru, K.S.; Ammunje, D.N.; Kannan, S.; Chandrasekaran, J.; et al. Aphrodisiac Performance of Bioactive Compounds from *Mimosa pudica* Linn.: In Silico Molecular Docking and Dynamics Simulation Approach. *Molecules* **2022**, *27*, 3799. [CrossRef] [PubMed]
38. Haider, M.; Elsherbeny, A.; Pittalà, V.; Fallica, A.N.; Alghamdi, M.A.; Greish, K. The Potential Role of Sildenafil in Cancer Management through EPR Augmentation. *J. Pers. Med.* **2021**, *11*, 585. [CrossRef] [PubMed]
39. Radwan, A.A. Pharmacophore elucidation and molecular docking studies on phosphodiesterase-5 inhibitors. *Bioinformation* **2015**, *11*, 63–66. [CrossRef] [PubMed]

40. Courvoisier, E.; Williams, A.P.; Lim, G.K.; Hughes, C.E.; Kenneth, D.M.H. The crystal structure of *L*-arginine. *Chem. Commun.* **2012**, *48*, 2761–2763. [CrossRef] [PubMed]
41. National Center for Biotechnology Information. PubChem Compound Summary for CID 4510, Nitroglycerin. Available online: https://pubchem.ncbi.nlm.nih.gov/compound/Nitroglycerin (accessed on 20 May 2026).
42. National Center for Biotechnology Information. PubChem Compound Summary for CID 135398744, Sildenafil. Available online: https://pubchem.ncbi.nlm.nih.gov/compound/Sildenafil (accessed on 20 May 2026).
43. Jendrzejewska, I.; Goryczka, T.; Pietrasik, E.; Klimontko, J.; Jampilek, J. Identification of Sildenafil Compound in Selected Drugs Using X-ray Study and Thermal Analysis. *Molecules* **2023**, *28*, 2632. [CrossRef] [PubMed]
44. Yathirajan, H.S.; Nagaraj, B.; Nagaraja, P.; Bolte, M. Sildenafil citrate monohydrate. *Acta Crystallogr. E.–Struct. Rep.* **2005**, *62*, o489–o491. [CrossRef]
45. Barbas, R.; Llinas, A.; Prohens, R. The Solid State Landscape of the Sildenafil Drug. *J. Pharm. Sci.* **2022**, *111*, 1104–1109. [CrossRef] [PubMed]
46. Banerjee, R.; Bhatt, P.M.; Desiraju, G.R. Solvates of Sildenafil Saccharinate. A New Host Material. *Cryst. Growth Des.* **2006**, *6*, 1468. [CrossRef]
47. Frisch, M.J.; Trucks, G.W.; Schlegel, H.B.; Scuseria, G.E.; Robb, M.A.; Cheeseman, J.R.; Scalmani, G.; Barone, V.; Petersson, G.A.; Nakatsuji, H.; et al. *Gaussian 16*, Revision C.01; Gaussian, Inc.: Wallingford, CT, USA, 2016.
48. Becke, D. Density-functional thermochemistry. III. The role of exact exchange. *J. Chem. Phys.* **1993**, *98*, 5648–5652. [CrossRef]
49. Wadt, W.R.; Hay, P.J. Ab initio effective core potentials for molecular calculations. Potentials for the transition metal atoms Sc to Hg. *J. Chem. Phys.* **1985**, *82*, 270–283. [CrossRef]
50. Wadt, W.R.; Hay, P.J. Ab initio effective core potentials for molecular calculations. Potentials for K to Au including the outermost core orbitals. *J. Chem. Phys.* **1985**, *82*, 299–310. [CrossRef]
51. Chemical Computing Group ULC. *Molecular Operating Environment (MOE)*, Version 2019.01; Chemical Computing Group: Montreal, QC, Canada, 2019. Available online: https://www.chemcomp.com/ (accessed on 20 May 2026).
52. Haga, K.; Kruse, A.C.; Asada, H.; Yurugi-Kobayashi, T.; Shiroishi, M.; Zhang, C.; Weis, W.I.; Okada, T.; Kobilka, B.K.; Haga, T.; et al. Structure of the human M2 muscarinic acetylcholine receptor bound to an antagonist. *Nature* **2012**, *482*, 547–551. [CrossRef] [PubMed]
53. Walsh, R.M.; Roh, S.H.; Gharpure, A.; Morales-Perez, C.L.; Teng, J.; Hibbs, R.E. Structural principles of distinct assemblies of the human α4β2 nicotinic receptor. *Nature* **2018**, *557*, 261–265. [CrossRef] [PubMed]
54. Sikakulya, F.K.; Ssebuufu, R.; Okedi, X.F.; Baluku, M.; Lule, H.; Kyamanywa, P. Open hemorrhoidectomy under local anesthesia versus saddle block in western Uganda: A study protocol for a prospective equivalence randomized, double-blind controlled trial. *Trials* **2022**, *23*, 652. [CrossRef] [PubMed]
55. Perek, A. Randomised comparison of the effect of 0.2% glyceryl trinitrate and 0.5% topical nifedipine in acute anal fissure treatment. *Turk. J. Colorectal Dis.* **2020**, *30*, 246–252. [CrossRef]
56. Faul, F.; Erdfelder, E.; Lang, A.G.; Buchner, A. G*Power 3: A flexible statistical power analysis program for the social, behavioral, and biomedical sciences. *Behav. Res. Methods* **2007**, *39*, 175–191. [CrossRef] [PubMed]
57. Potdar, R.P.; Khollam, Y.B.; Shaikh, S.F.; More, P.S.; Rana, A.u.H.S. Polyvinylpyrrolidone-capped silver nanoparticles for highly sensitive and selective optical fiber-based ammonium sensor. *Nanomaterials* **2022**, *12*, 3373. [CrossRef] [PubMed]
58. Melnikov, P.; Corbi, P.P.; Cuin, A.; Cavicchioli, M.; Guimarães, W.R. Physicochemical properties of sildenafil citrate (Viagra) and sildenafil base. *J. Pharm. Sci.* **2003**, *92*, 2140–2143. [CrossRef] [PubMed]
59. Jin, J.Z.; Bhat, S.; Park, B.; Hardy, M.O.; Unasa, H.; Mauiliu-Wallis, M.; Hill, A.G. A systematic review and network meta-analysis comparing treatments for anal fissure. *Surgery* **2022**, *172*, 41–52. [CrossRef] [PubMed]
60. Hwang, S.H. Trends in treatment for hemorrhoids, fistula, and anal fissure: Go along the current trends. *J. Anus Rectum Colon* **2022**, *6*, 150–158. [CrossRef] [PubMed]
61. Salem, A.E.; Mohamed, E.A.; Elghadban, H.M.; Abdelghani, G.M. Potential combination topical therapy of anal fissure: Development, evaluation, and clinical study. *Drug Deliv.* **2018**, *25*, 1672–1682. [CrossRef] [PubMed]
62. Nevins, E.J.; Kanakala, V. Topical diltiazem and glyceryl-trinitrate for chronic anal fissure: A meta-analysis of randomized controlled trials. *Turk. J. Surg.* **2020**, *36*, 347–352. [CrossRef] [PubMed]
63. Medici, S.; Peana, M.; Crisponi, G.; Nurchi, V.M.; Lachowicz, J.I.; Remelli, M.; Zoroddu, M.A. Silver coordination compounds: A new horizon in medicine. *Coord. Chem. Rev.* **2016**, *327–328*, 349–359. [CrossRef]
64. Hasan, R.; Alshammari, A.; Albekairi, N.A.; Bhuia, M.S.; Afroz, M.; Chowdhury, R.; Khan, M.A.; Ansari, S.A.; Ansari, I.A.; Mubarak, M.S.; et al. Antiemetic activity of abietic acid possibly through the 5HT3 and muscarinic receptors interaction pathways. *Sci. Rep.* **2024**, *14*, 6642. [CrossRef] [PubMed]
65. Chowdhury, R.; Bhuia, M.S.; Rakib, A.I.; Hasan, R.; Coutinho, H.D.M.; Araújo, I.M.; de Menezes, I.R.A.; Islam, M.T. Assessment of Quercetin Antiemetic Properties: In Vivo and In Silico Investigations on Receptor Binding Affinity and Synergistic Effects. *Plants* **2023**, *12*, 4189. [CrossRef] [PubMed]

66. Situ, S.G.; Bhuia, M.S.; Chowdhury, R.; Al Hasan, S.; Ansari, S.A.; Ansari, I.A.; Ali, A.; Islam, M.T. Synergistic Antiemetic Effects of Nerolidol on Domperidone, Hyoscine, and Ondansetron: In Vivo and in Silico Investigations on Receptor Binding Affinity. *ChemistryOpen* **2025**, *14*, e202400345. [CrossRef]
67. Alpaslan, M.K.; Rouzi, K.; Poyraz, E.B.; Dege, N.; Bouatia, M.; El Karbane, M.; Karrouchi, K. Synthesis, crystal structure, and molecular docking analysis of 1-(3-(2-chlorophenyl)-4,5-dihydroisoxazol-5-yl) pyrrolidin-2-one: Insights into biological interactions and drug design. *J. Mol. Struct.* **2025**, *1347*, 143354. [CrossRef]
68. Kulshreshtha, M.; Sharma, A.K.; Pathak, D.; Pandey, P.; Snehi, V.; Shukla, K.S.; Ved, A.; Singh, A.; Verma, N.; Singh, A.; et al. Cardioprotective Potential of *Qusqualis indica* Leaves; An in silico Docking Study. *Free Rad. Antiox.* **2023**, *13*, 41–45. [CrossRef]
69. Kanasuwan, A.; Deuther-Conrad, W.; Chongruchiroj, S.; Sarasamkan, J.; Chotipanich, C.; Vajragupta, O.; Arunrungvichian, K. Selective $\alpha_3\beta_4$ Nicotinic Acetylcholine Receptor Ligand as a Potential Tracer for Drug Addiction. *Int. J. Mol. Sci.* **2023**, *24*, 3614. [CrossRef] [PubMed]
70. Grillberger, K.; Cöllen, E.; Trivisani, C.I.; Blum, J.; Leist, M.; Ecker, G.F. Structural Insights into Neonicotinoids and *N*-Unsubstituted Metabolites on Human nAChRs by Molecular Docking, Dynamics Simulations, and Calcium Imaging. *Int. J. Mol. Sci.* **2023**, *24*, 13170. [CrossRef] [PubMed]
71. Gaona, J.; Gadekar, P.K.; Abdelwahed, K.S.; Sanchez, N.E.; Rolling, A.; Beaudoin, R.; Bill, B.; Kerr, A.T.; Thakur, G.A.; Hamouda, A.K. Enantiospecific Positive Allosteric Modulation of $\alpha4\beta2$ Nicotinic Receptor Subtypes. *ACS Chem. Neurosci.* **2025**, *16*, 1937–1950. [CrossRef] [PubMed]
72. Thasweer, A.M.; Devi, P.R.; Thirunavukkarasu, V. Molecular docking and dynamic simulation studies of α4β2 and α7 nicotinic acetylcholine receptors with tobacco smoke constituents nicotine, NNK and NNN. *J. Biomol. Struct. Dynam.* **2022**, *41*, 8462–8471. [CrossRef] [PubMed]

Disclaimer/Publisher's Note: The statements, opinions and data contained in all publications are solely those of the individual author(s) and contributor(s) and not of MDPI and/or the editor(s). MDPI and/or the editor(s) disclaim responsibility for any injury to people or property resulting from any ideas, methods, instructions or products referred to in the content.